

Multi-point Infection Dynamics of Hepatitis B in the Presence of Sub-Viral Particles

Rupchand Sutradhar, Gopinath Sadhu and D C Dalal
Indian Institute of Technology Guwahati, Guwahati, Assam, India, 781039

1 Abstract

Hepatitis B virus (HBV) is considered as etiological agent of the lethal liver disease hepatitis B. Globally, hepatitis B is recognized as one of the prevailing infectious diseases with a significant impact on human health. In spite of being non-infectious in nature, sub-viral particles (SVPs), composed with mainly viral surface proteins, play critical roles in the persistence and progression of the infection. Although the understanding on the functions of these non-infectious SVPs remains limited and incomplete. In this study, a mathematical model is proposed for the first time by incorporating the roles of SVPs and including the effects of capsids recycling. The impacts of spatial mobility of capsids, viruses, SVPs and antibodies are also taken into account in this model. Overall, this model carry unique characteristics in the context of this viral infection. This study investigates the changes in the dynamics of infection considering both single-point as well as multi-point infection initial condition. As a result, it is observed that SVPs can significantly enhance intracellular viral replication and gene expression by reducing the neutralization of virus particles by antibodies. The recycling of capsids substantially increase the concentration of SVPs. The experiments which are carried out on single-point as well as multi-point infection initial conditions show that if the liver is infected at more than one point, infection propagates rapidly. The outcomes of the proposed model strongly recommend that it is imperative to consider the diffusion term while HBV infection dynamics are illustrated.

Keywords: Hepatitis B; Sub-viral particles; Mathematical model; Diffusion; Multi-point infection; Numerical simulation

2 Introduction

Hepatitis B virus (HBV) represents a significant and formidable threat to human health throughout the world with ample potential to cause life-threatening consequences. This viral infection infiltrates the liver, leading to a wide spectrum of outcomes that can extend from acute illness to chronic infection, and in some cases, even to fatal complications like hepatocellular carcinoma (HCC) [1]. The insidious nature of HBV lies in its ability to silently persist within the host body, quietly replicating and damaging liver cells over an extended period of time. Left untreated or undiagnosed, chronic HBV infection can progress to severe conditions such as liver cirrhosis where the liver becomes scarred and loses its functionality, ultimately resulting liver failure. The devastating impacts of HBV on individuals and communities emphasize the urgent need for widespread awareness, vaccination, early diagnosis, and access to effective treatment interventions to mitigate this life-threatening consequences.

Over the past two decades, many authors have been diligently researching HBV infections from different angles [2–6]. The primary causes for the persistence of this infection include the high stability of cccDNAs, the intricate life cycle of the virus, and the crucial functions played by certain viral components, such as HBx proteins, surface proteins (L/M/SHBs), sub-viral particles (SVPs), and many more. SVPs which are produced by HBV infected cells during infection period

are non-infectious in nature. These are predominantly composed of viral surface antigens (HBsAg) proteins that are the major components of the lipid bilayer envelope [7]. SVPs don't contain nucleocapsid proteins and viral nucleic acids, *i.e.*, lack the rcDNA-containing capsids or the viral genome. The production of SVPs is a natural biological process. While the viruses replicate within the hepatocytes (liver cells), both complete viral particles and SVPs produce simultaneously and release into the bloodstream. Generally, SVPs are found in the blood of infected individuals in two main forms: (i) spherical particles measuring 25 nm in diameter and (ii) filaments with a diameter of 22 nm which can differ in length [8, 9]. In the literature, many authors have reported that the ratio of Dane particles to SVPs ranges from 1:10,000 to 1:100,000 [9–11], *i.e.*, a large quantity of HBsAg derived from viral particles has no effect on the reservoir of viral replication. Although, the actual reasons behind their overproduction and their exact roles in HBV pathogenesis are still under investigation [12]. The assembly and secretion pathways for SVPs are typically distinct from those used by the virus. Researchers are dedicated to unravel the primary causes underlying their excessive production and understand their critical functions in the development of HBV-related illnesses. In individuals with chronic HBV infection, the number of SVPs far surpasses that of infectious virions in the bloodstream. To the best of our knowledge, despite its significant overproduction, the functions of SVPs have been widely overlooked in the previous studies [5, 6, 13–24], leaving a gap in our knowledge about their biological importance. Recently, Cao et al. [25] demonstrated the distribution of Dane particles (virus), spherical particles, and filamentous particles using micrographs and suggested that there is a universal folding shape of HBsAg on SVPs. From the perspective of Rydell et al. [25, 26], SVPs are believed to potentially facilitate cell-to-cell spread, particularly in the presence of neutralizing antibodies. SVPs function as a disguise for the virus. As a result of this characteristic of SVPs, a substantial portion of HBV-specific antibodies produced by the host's immune system is targeted towards neutralizing SVPs, thereby helping the virus evade the immune response [26]. However, to the best of our knowledge, this effect has not been demonstrated experimentally or in animal models so far. Although, SVPs are less efficient in blocking viral entry by binding to target cells [27]. High levels of SVPs can stimulate the immune system, leading to the production of antibodies against HBsAg. For this virus, Bruns et al. [28], and Klingmüller and Schaller [29] reported that SVPs have capability to both enhance and inhibit cell attachment of the virus. The collective evidence suggests that SVPs have some notable impacts on the advancement and perpetuation of the infection. Based on these findings, it is apparent that more elaborate studies are imperative to enhance understanding about SVPs.

The propagation of viral particles both between and within the hosts is inherently a spatial process. Diffusion plays a pivotal role in viral infection by facilitating the spread of viral particles both locally within the liver and systemically throughout the body. This diffusion also impacts the immune response, as SVPs diffuses widely, potentially diverting immune attention from infectious virions and contributing to immune evasion. Some researchers have already addressed how spatial heterogeneity influences the dynamics of infection of certain viruses, such as HIV [30], Covid-19 [31], etc. In case of HBV infection, a number of studies [32–34] have also been documented the effects of diffusion of virus particles in the literature. However, none of these studies have simultaneously taken into account the effects of capsid recycling, the roles of SVPs, and the functions of antibodies. Recently, Sutradhar and Dalal [24, 35] have explored the impacts of capsid recycling on HBV infection and found that the cytoplasmic recycling of rcDNA-containing capsids enhances the infection. So, it is important to consider capsid recycling while studying HBV infection.

Motivated by the aforementioned discussion, in this study, we shed light on the roles of SVPs in the development of infection via a modified HBV infection dynamics model. In this framework, incorporating the diffusion of capsids, virus, SVPs and antibodies, and the impacts of SVPs, we extend our previously proposed HBV infection dynamics model mentioned in the article [35]. The precise interplay between virus particles and antibodies is also focused on this work. In this immediate version, it is considered that the capsids, viruses, SVPs and antibodies follow the Fickian diffusion that refers to the process of molecular or particle transport driven by concen-

tration gradients, described by Fick’s laws of diffusion. The influences of the spatial diffusion of capsids, viruses, SVPs, and antibodies will be also explained from different perspectives. On the other hand, the initial conditions of the infection are another key factor that significantly affects the infection’s dynamics. It is also aimed to investigate the correlations between outcomes of the infection and various types of initial conditions, such as single-origin, dual-origin, triple-origin, etc. Here, “ n -origin” initial conditions indicate that the infection originates from n distinct points within the liver. The following are the main contributions of this study:

- The roles of SVPs on HBV infection.
- The impacts spatial mobility of HBV DNA-containing capsids, viruses, SVPs and antibodies.
- The effects of capsid recycling on the production of SVPs.
- Dysfunction of antibody in the presence of SVPs.
- Dual-origin and triple-origin infection: Unraveling the dynamics of infection.

3 Formulation of model based on existing literature

In the last three decades, extensive research has been carried out with the goal of eradicating HBV infection and ensuring human well-being. Many researchers have proposed different mathematical models to study the spread of infection. Each model was designed with a specific objective and pursued in a distinct direction [5, 6, 18–24]. For example, Sutradhar and Dalal [35] recently studied the effects of capsid recycling in HBV infection by proposing the following HBV infection dynamics model (with slight symbolic modification):

$$\begin{aligned}
 \frac{dX(t)}{dt} &= \lambda - \mu X(t) - kV(t)X(t), \\
 \frac{dY(t)}{dt} &= kV(t)X(t) - \delta Y(t), \\
 \frac{dU(t)}{dt} &= aY(t) + \gamma(1 - \eta)U(t) - \eta\beta U(t) - \delta U(t), \\
 \frac{dV(t)}{dt} &= \eta\beta U(t) - \delta_v V(t).
 \end{aligned} \tag{1}$$

The temporal change of each component of this proposed model (1) is determined based on the mass action principle. Here, the variables $X(t)$, $Y(t)$, $U(t)$, and $V(t)$ are ascribed to the specific compartment of the system of equations (1), representing uninfected hepatocytes, infected hepatocytes, rcDNA-containing capsids, and viruses, respectively. Uninfected hepatocytes are assumed to be produced with the natural growth rate of λ and degraded with natural death rate μ . It is considered that the infectious virus particles have the capability to infect the uninfected hepatocytes at a rate of k . The parameter a denotes the production rate of capsids from infected hepatocytes. Within this model (1), η fraction of the capsids is assumed to give birth of new viruses with a production rate of β . On the other hand, the remaining portion of the capsids is returned to the nucleus at a rate γ to increase the pool of covalently closed circular DNA (cccDNA). The process where newly produced capsids go back to the nucleus is termed “recycling of capsids”, with γ representing the recycling rate. Both infected hepatocytes and capsids undergo natural decay at a common death rate δ . The parameter, δ_v denotes the spontaneous clearance rate of viruses.

In order to extend the above model (1), authors of this article incorporate the functions of SVPs and antibodies through the introduction of two distinct additional classes, namely SVPs and antibodies. It is believed that the diffusion of viral components plays a pivotal role in controlling and preventing infection. The effects of spatial mobility of all viral components (rcDNA-containing capsids, viruses, SVPs) and antibodies are also taken into account to make the model more reliable and closer to reality.

3.1 Governing equations

The mathematical formulation of the model is as follows:

$$\frac{\partial X(x, t)}{\partial t} = \lambda - \mu X(x, t) - kV(x, t)X(x, t), \quad \text{in } \Omega \times (0, \tau), \quad (2)$$

$$\frac{\partial Y(x, t)}{\partial t} = kV(x, t)X(x, t) - \delta Y(x, t), \quad \text{in } \Omega \times (0, \tau), \quad (3)$$

$$\frac{\partial U(x, t)}{\partial t} = \mathcal{D}_1 \frac{\partial^2 U(x, t)}{\partial x^2} + aY(x, t) + \gamma(1 - \alpha)U(x, t) - \alpha\beta U(x, t) - \delta U(x, t), \quad \text{in } \Omega \times (0, \tau), \quad (4)$$

$$\frac{\partial V(x, t)}{\partial t} = \mathcal{D}_2 \frac{\partial^2 V(x, t)}{\partial x^2} + \alpha\beta U(x, t) - g_1 A(x, t)V(x, t) - \delta_v V(x, t), \quad \text{in } \Omega \times (0, \tau), \quad (5)$$

$$\frac{\partial S_v(x, t)}{\partial t} = \mathcal{D}_3 \frac{\partial^2 S_v(x, t)}{\partial x^2} + bY(x, t) - g_2 A(x, t)S_v(x, t) - \delta_s S_v(x, t), \quad \text{in } \Omega \times (0, \tau), \quad (6)$$

$$\begin{aligned} \frac{\partial A(x, t)}{\partial t} = & \mathcal{D}_4 \frac{\partial^2 A(x, t)}{\partial x^2} + h(V(x, t) + S_v(x, t)) + r_A A(x, t) \left(1 - \frac{A(x, t)}{A_m}\right) - g_1 A(x, t)V(x, t) \\ & - g_2 A(x, t)S_v(x, t) - \delta_a A(x, t), \quad \text{in } \Omega \times (0, \tau), \end{aligned} \quad (7)$$

where $\Omega \subset \mathbb{R}$ is a bounded domain where viruses, cells and antibodies stay and can interact. Here, $X(x, t)$, $Y(x, t)$, $U(x, t)$, $V(x, t)$, $S_v(x, t)$ and $A(x, t)$ represent uninfected cells, infected cells, rcDNA-containing capsids, viruses, SVPs, and antibodies at the point $(x, t) \in \Omega \times (0, \tau)$, respectively. The physical meaning of the parameters $\lambda, \mu, k, \delta, a, \gamma, \eta, \beta, \delta_v$ are the same as those in model (1). We adhere to the fact that uninfected and infected hepatocytes do not exhibit any kind of spatial movement. The corresponding spatial mobilities of capsids, viruses, SVPs, and antibodies in the liver are characterized by diffusion coefficients $\mathcal{D}_1, \mathcal{D}_2, \mathcal{D}_3$, and \mathcal{D}_4 . The proposed model (equations (2)-(7)) will be called *diffusion model* if the value of any \mathcal{D}_i , $i = 1, 2, 3, 4$ is non-zero. Otherwise, this model will be addressed as *non-diffusion model*. The parameters b denote the production rate of SVPs from infected hepatocytes. In general, $b \gg a$ since infection with HBV results in the synthesis of a large number of SVPs, likely at least 1,000-fold more than virus particles [36]. It is considered that the development of antibodies is equally influenced by the presence of both virions and SVPs. The term $h(V(x, t) + S_v(x, t))$ reflects the production of antibodies whereas h denotes the production rate of antibodies following the work done by Ciupe et al. [37]. Since both virions and SVPs display the HBV-specific antigen on their surface, antibodies are equally effective in neutralizing both types, thereby providing a robust immune response against infection. The neutralizing rate of viruses is given by $g_1 A(x, t)V(x, t)$ as described in the article of Chenar et al. [38], where g_1 represent the association rate constant for antibodies reacting to viral. The SVPs are also inactivated by direct binding with antibodies, which is represented by the term $g_2 A(x, t)S_v(x, t)$ in the model [37, 39]. The parameter δ_s and δ_a denote the normal decay rates of SVPs and antibodies, respectively. In the absence of the virus, we also introduce a logistic term with a maximum intrinsic growth rate r_A and a carrying capacity A_m for the maintenance of antibodies through homeostasis. This term ensures that the antibody population grows to a stable level, reflecting the natural homeostatic control mechanisms within the immune system. In a nutshell, the semantic representation of the above proposed model (equations (2)-(7)) are shown in the Figure 1. This model encompasses numerous biological phenomena and can be regarded as more generalized than existing models.

3.2 Initial and boundary conditions

In order to close the system (equation (2)-(7)), it is essential to specify reasonable initial and boundary conditions for each compartment ($X(x, t), Y(x, t), U(x, t), V(x, t), S_v(x, t)$, and $A(x, t)$) of the proposed model. For the convenience of analysis, let L be the total length of the liver shown in Figure 2 and $[0, L]$ be the domain of interest. We denote $[0, L]$ as Ω . It is assumed that the infection initially starts from $x = 0$, *i.e.*, from the left side of the liver.

- **Initial conditions:**

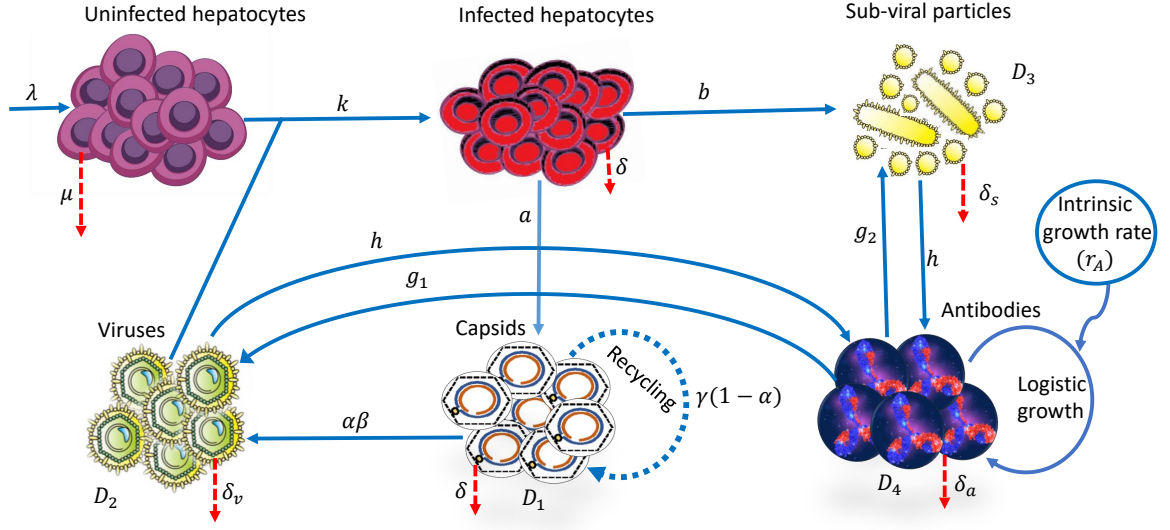


Figure 1: Semantic representation of the proposed model given by the system of equations (2)-(7).

For defining the initial conditions for each model compartment in the domain $[0, L]$, we adhere to the following biologically relevant assumptions:

1. At the point of infection (POI) $x = 0$, the concentration of uninfected hepatocytes is very low, whereas the concentration of infected hepatocytes is extremely high.
2. At the POI, the initial concentrations of HBV capsids, viruses, SVPs and antibodies are maximum and equal for all, *i.e.*, $D_0 = V_0 = S_{v0} = A_0$.

Following the similar approach as detailed in the article of Chaplain and Lolas [40], the respective initial conditions are formulated. In terms of mathematics, the initial concentrations are written in equation (8) and are visualized in Figure 3.

$$\begin{aligned}
 X(x, 0) &= M \left\{ 1 - \exp\left(-\frac{x^2}{\epsilon}\right) \right\}, \quad 0 \leq x \leq L, \\
 Y(x, 0) &= M \exp\left(-\frac{x^2}{\epsilon}\right), \quad 0 \leq x \leq L, \\
 U(x, 0) &= U_0 \exp\left(-\frac{x^2}{\epsilon}\right), \quad 0 \leq x \leq L, \\
 V(x, 0) &= V_0 \exp\left(-\frac{x^2}{\epsilon}\right), \quad 0 \leq x \leq L, \\
 S_v(x, 0) &= S_{v0} \exp\left(-\frac{x^2}{\epsilon}\right), \quad 0 \leq x \leq L, \\
 A(x, 0) &= A_0 \exp\left(-\frac{x^2}{\epsilon}\right), \quad 0 \leq x \leq L, \quad \text{with } \epsilon = 0.01.
 \end{aligned} \tag{8}$$

Guided by the in vivo protocol in which infection takes place within the liver, it is assumed that there is no-flux of capsids, viruses, SVPs and antibodies across the boundary of the liver, *i.e.*, throughout the infection, the liver acts as an impregnable fortress, forbidding the entry or exit of any particles. The end points of the liver are denoted by $x = 0$ and $x = L$ in one-dimensional framework, shown in Figure 2. These imposed homogeneous Neumann boundary conditions are

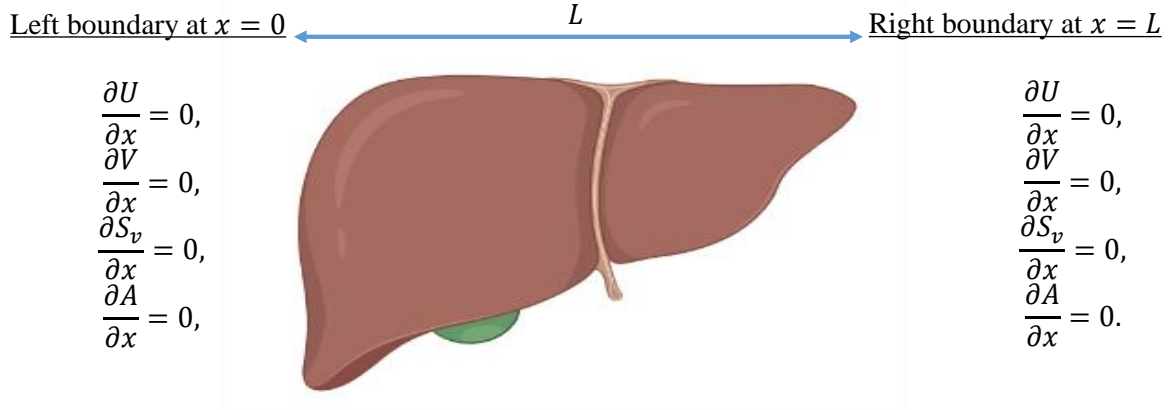


Figure 2: The length of the liver and the prescribed boundary conditions at $x = 0$ and $x = L$ are shown at the left and right sides of the liver, respectively. This picture of liver is taken from BioRender.com.

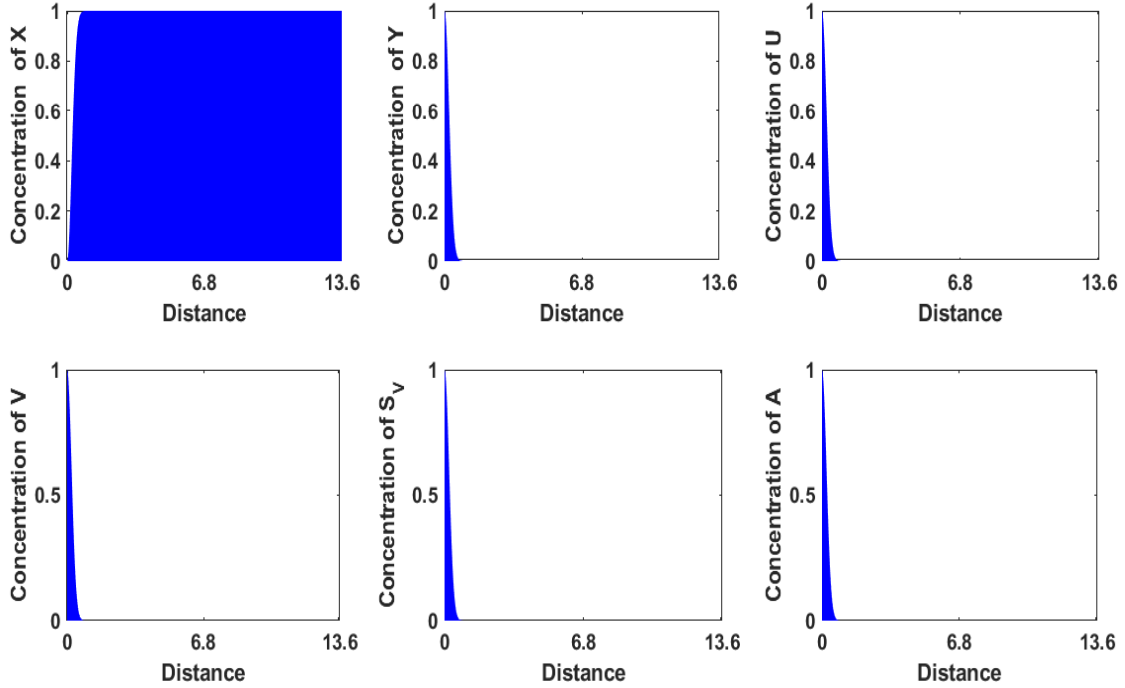


Figure 3: The graphical representation of all initial conditions mentioned in the equation (8).

represented by the following equations;

$$\frac{\partial U(x, t)}{\partial x} \Big|_{x=0} = \frac{\partial V(x, t)}{\partial x} \Big|_{x=0} = \frac{\partial S_v(x, t)}{\partial x} \Big|_{x=0} = \frac{\partial A(x, t)}{\partial x} \Big|_{x=0} = 0, \quad t \geq 0, \quad (9)$$

and

$$\frac{\partial U(x, t)}{\partial x} \Big|_{x=L} = \frac{\partial V(x, t)}{\partial x} \Big|_{x=L} = \frac{\partial S_v(x, t)}{\partial x} \Big|_{x=L} = \frac{\partial A(x, t)}{\partial x} \Big|_{x=L} = 0, \quad t \geq 0, \quad (10)$$

where $\frac{\partial}{\partial x}$ denotes the outward normal derivative on the boundary of the domain $x = 0$ and $x = L$.

Note: For simplicity, $X, Y, U, V, S_v,$ and A will be used instead of expressions $X(x, t), Y(x, t), U(x, t), V(x, t), S_v(x, t),$ and $A(x, t)$ throughout the rest of this study.

4 Non-dimensional form of the proposed model

Due to the presence of high non-linearity in the proposed model problem, the system of PDEs (equation (2)-(7)) is solved numerically. In order to do non-dimensionalization of the proposed model, the following typical scales are used:

- (1) Reference length scale, L , is chosen to be the total length of the liver along the x -direction. The approximate value of L is considered as $L = 13.6$ cm [41].
- (2) Using \mathcal{D}_l , time scale can be written as $\bar{t} = \frac{L^2}{\mathcal{D}_l}$, where \mathcal{D}_l is a reference chemical diffusion coefficient,
- (3) It is considered that the total number of liver cells is denoted by $M = 2 \times 10^{11}$ [42].
- (4) Initially, maximum values of concentration of capsids D_0 , viruses V_0 , SVPs S_0 , antibodies A_0 , are attained at the point of infection $x = 0$.

By using these scales, the following non-dimensional variables and parameters are obtained as follows:

- **Dimensionless model variables:** $t^* = \frac{t}{\bar{t}}$, $x^* = \frac{x}{L}$, $Y^* = \frac{Y}{M}$, $X^* = \frac{X}{M}$, $U^* = \frac{U}{U_0}$, $V^* = \frac{V}{V_0}$, $S^* = \frac{S_v}{S_{v0}}$ and $A^* = \frac{A}{A_0}$.
- **Dimensionless model parameters:** $\lambda^* = \frac{\bar{t}\lambda}{M}$, $\mu^* = \mu\bar{t}$, $k^* = kV_0\bar{t}$, $\delta^* = \delta\bar{t}$, $a^* = \frac{aM\bar{t}}{U_0}$, $\gamma^* = \gamma\bar{t}$, $\beta^* = \beta\bar{t}$, $g^* = gA_0\bar{t}$, $\delta_v^* = \delta_v\bar{t}$, $b^* = \frac{b\bar{t}M}{S_{v0}}$, $\delta_s^* = \delta_s\bar{t}$, $\delta_a^* = \delta_a\bar{t}$, $h^* = h\bar{t}$, $r_a^* = r_A\bar{t}$, $A_m^* = \frac{A_m}{A_0}$, $\mathcal{D}_1^* = \frac{\mathcal{D}_1}{\mathcal{D}_l}$, $\mathcal{D}_2^* = \frac{\mathcal{D}_2}{\mathcal{D}_l}$, $\mathcal{D}_3^* = \frac{\mathcal{D}_3}{\mathcal{D}_l}$, $\mathcal{D}_4^* = \frac{\mathcal{D}_4}{\mathcal{D}_l}$.

At first, the equations (2)-(7) are non-dimensionalized using the aforementioned dimensionless variables and parameters. For the sake of notational simplicity and clarity, omitting the star (*) from each dimensionless variable and parameter, the non-dimensional governing equations are derived to be:

$$\frac{\partial X}{\partial t} = \lambda - \mu X - kVX, \quad (11)$$

$$\frac{\partial Y}{\partial t} = kVX - \delta Y, \quad (12)$$

$$\frac{\partial U}{\partial t} = \mathcal{D}_1 \frac{\partial^2 U}{\partial x^2} + aY + \gamma(1 - \alpha)U - \alpha\beta U - \delta U, \quad (13)$$

$$\frac{\partial V}{\partial t} = \mathcal{D}_2 \frac{\partial^2 V}{\partial x^2} + \alpha\beta U - gAV - \delta_v V, \quad (14)$$

$$\frac{\partial S_v}{\partial t} = \mathcal{D}_3 \frac{\partial^2 S_v}{\partial x^2} + bY - gAS_v - \delta_s S_v, \quad (15)$$

$$\frac{\partial A}{\partial t} = \mathcal{D}_4 \frac{\partial^2 A}{\partial x^2} + h(V + S_v) + r_A A \left(1 - \frac{A}{A_m}\right) - gA(S_v + V) - \delta_a A. \quad (16)$$

Due to the non-dimensionalization, the domain of interest $[0, L]$ transforms to $[0, 1]$. The initial and boundary conditions take the following form in the domain $[0, 1]$:

- **Non-dimensional form of initial conditions:**

$$\left. \begin{aligned} X(x, 0) &= 1 - \exp\left(-\frac{x^2}{\epsilon}\right), \quad 0 \leq x \leq 1, \\ Y(x, 0) &= \exp\left(-\frac{x^2}{\epsilon}\right), \quad 0 \leq x \leq 1, \\ U(x, 0) &= \exp\left(-\frac{x^2}{\epsilon}\right), \quad 0 \leq x \leq 1, \\ V(x, 0) &= \exp\left(-\frac{x^2}{\epsilon}\right), \quad 0 \leq x \leq 1, \\ S_v(x, 0) &= \exp\left(-\frac{x^2}{\epsilon}\right), \quad 0 \leq x \leq 1, \\ A(x, 0) &= \exp\left(-\frac{x^2}{\epsilon}\right), \quad 0 \leq x \leq 1. \end{aligned} \right\} \quad (17)$$

- **Non-dimensional form of boundary conditions:**

$$\frac{\partial U}{\partial x} = \frac{\partial V}{\partial x} = \frac{\partial S_v}{\partial x} = \frac{\partial A}{\partial x} = 0 \quad \text{on } \partial\Omega^* \times (0, +\infty), \quad (18)$$

where $\partial\Omega^*$ represents boundary of $\Omega^* = [0, 1]$ and $(0, +\infty)$ denotes the temporal domain.

5 Numerical method

The computational domain $[0, 1]$ is divided into $(N - 1)$ equal sub-intervals $0 = x_0 \leq x_1 \leq x_2 \leq \dots \leq x_{i-1} \leq x_i \leq x_{i+1} \leq \dots \leq x_{N-2} \leq x_{N-1} = 1$ with step length $\Delta x = \frac{1}{(N - 1)}$. Let Δt be the time step length and n be the step number to reach the final time T_f i.e., $T_f = n\Delta t$. Here, the central difference scheme for spatial derivatives and the forward scheme for temporal derivatives (FTCS) is used to discretize the governing equations (11)-(16). Using the following notations:

$$\begin{aligned} X(x, t) &= X(i\Delta x, n\Delta t) = X_i^n, \\ Y(x, t) &= Y(i\Delta x, n\Delta t) = Y_i^n, \\ U(x, t) &= U(i\Delta x, n\Delta t) = U_i^n, \\ V(x, t) &= V(i\Delta x, n\Delta t) = V_i^n, \\ S_v(x, t) &= S_v(i\Delta x, n\Delta t) = S_{v_i}^n, \\ A(x, t) &= A(i\Delta x, n\Delta t) = A_i^n, \end{aligned}$$

the corresponding discretized forms of the equations (11)-(16) at the interior nodes can be written as

$$X_i^{n+1} = X_i^n + \lambda\Delta t - \mu\Delta t X_i^n - k\Delta t V_i^n X_i^n, \quad (19)$$

$$Y_i^{n+1} = Y_i^n - \delta\Delta t Y_i^n + k\Delta t V_i^n X_i^n, \quad (20)$$

$$-p_1 U_{i-1}^{n+1} + (1 + 2p_1) U_i^{n+1} - p_1 U_{i+1}^{n+1} = U_i^n + a\Delta t Y_i^n + \gamma\Delta t (1 - \alpha) U_i^n - \alpha\beta\Delta t U_i^n - \delta\Delta U_i^n, \quad (21)$$

$$-p_2 V_{i-1}^{n+1} + (1 + 2p_2) V_i^{n+1} - p_2 V_{i+1}^{n+1} = V_i^n + \alpha\beta\Delta t U_i^n - g\Delta t A_i^n V_i^n - \delta_v\Delta t V_i^n, \quad (22)$$

$$-p_3 S_{v_{i-1}}^{n+1} + (1 + 2p_3) S_{v_i}^{n+1} - p_3 S_{v_{i+1}}^{n+1} = S_{v_i}^n + b\Delta t Y_i^n - g\Delta t S_{v_i}^n A_i^n - \delta_s\Delta t S_{v_i}^n, \quad (23)$$

$$-p_4 A_{i-1}^{n+1} + (1 + 2p_4) A_i^{n+1} - p_4 A_{i+1}^{n+1} = A_i^n + (h - gA_i^n)(S_{v_i}^n + V_i^n) + r_A A_i^n \left(1 - \frac{A_i^n}{A_m}\right) - \delta_a\Delta t A_i^n, \quad (24)$$

where $i = 1, 2, \dots, N - 2, n = 0, 1, 2, \dots$. Here, $p_1 = \frac{\Delta t}{\Delta x^2} \mathcal{D}_1$, $p_2 = \frac{\Delta t}{\Delta x^2} \mathcal{D}_2$, $p_3 = \frac{\Delta t}{\Delta x^2} \mathcal{D}_3$, $p_4 = \frac{\Delta t}{\Delta x^2} \mathcal{D}_4$. Using ghost point criteria at the boundary nodes, *i.e.*, $i = 0$, and $i = N - 1$, equations (21), (22), (23) and (24) take the following forms:

- **At left boundary ($x = 0$):**

$$(1 + 2p_1)U_0^{n+1} - 2p_1U_1^{n+1} = U_0^n + a\Delta tY_0^n + \gamma\Delta t(1 - \alpha)U_0^n - \alpha\beta\Delta tU_0^n - \delta\Delta U_0^n, \quad (25)$$

$$(1 + 2p_2)V_0^{n+1} - 2p_2V_1^{n+1} = V_0^n + \alpha\beta\Delta tU_0^n - g\Delta tA_0^nV_0^n - \delta_v\Delta tV_0^n, \quad (26)$$

$$(1 + 2p_3)S_{v0}^{n+1} - 2p_3S_{v1}^{n+1} = S_{v0}^n + b\Delta tY_0^n - g\Delta tS_{v0}^nA_0^n - \delta_s\Delta tS_{v0}^n, \quad (27)$$

$$(1 + 2p_4)A_0^{n+1} - 2p_4A_1^{n+1} = A_0^n + (h - gA_0^n)(S_{v0}^n + V_0^n) + r_AA_0^n \left(1 - \frac{A_0^n}{A_m}\right) - \delta_a\Delta tA_0^n. \quad (28)$$

- **At right boundary ($x = 1$):**

$$-2p_1U_{N-2}^{n+1} + (1 + 2p_1)U_{N-1}^{n+1} = U_{N-1}^n + a\Delta tI_{N-1}^n + \gamma\Delta t(1 - \alpha)U_{N-1}^n - \alpha\beta\Delta tU_{N-1}^n - \delta\Delta U_{N-1}^n, \quad (29)$$

$$-2p_2V_{N-2}^{n+1} + (1 + 2p_2)V_{N-1}^{n+1} = V_{N-1}^n + \alpha\beta\Delta tU_{N-1}^n - g\Delta tA_{N-1}^nV_{N-1}^n - \delta_v\Delta tV_{N-1}^n, \quad (30)$$

$$-2p_3S_{vN-2}^{n+1} + (1 + 2p_3)S_{vN-1}^{n+1} = S_{vN-1}^n + b\Delta tY_{N-1}^n - g\Delta tS_{vN-1}^nA_i^n - \delta_s\Delta tS_{vN-1}^n, \quad (31)$$

$$\begin{aligned} -2p_4A_{N-2}^{n+1} + (1 + 2p_4)A_{N-1}^{n+1} &= A_{N-1}^n + (h - gA_{N-1}^n)(S_{vN-1}^n + V_{N-1}^n) \\ &+ r_AA_{N-1}^n \left(1 - \frac{A_{N-1}^n}{A_m}\right) - \delta_a\Delta tA_{N-1}^n. \end{aligned} \quad (32)$$

The corresponding systems of equations for U , V , S_v and A are solved using the well-known tridiagonal matrix algorithm (TDMA).

6 Parameter estimation

The baseline values of some parameters are directly taken from existing literature. It is assumed that the infectious viral particles and SVPs degrade naturally with same rate, *i.e.*, $\delta_v = \delta_s$. The value of volume fraction of rcDNA-containing capsids (α) in favor of virus production are considered as 0.8 throughout this study. Since, the ratio of Dane particles to SVPs ranges from 1:10,000 to 1:100,000 [9–11], it is noted that the production rate of SVPs is accounted to be at least 1000 times that of virus production rate, *i.e.*, $b = 1000a$. The diffusion coefficients ($\mathcal{D}_1, \mathcal{D}_2, \mathcal{D}_3, \mathcal{D}_4$) are systematically varied within a realistic range to capture the diverse spectrum of viral infection dynamics. All details regarding the parameters, such as descriptions, units, values, and their corresponding references are mentioned in Table 1.

7 Numerical experiment

By applying the methodology described in Section 5, the dimensionless system of equations (11)–(16) is solved considering the above-mentioned initial conditions (17) and boundary conditions (18). However, for the sake of illustration, the obtained results are presented in dimensional form to provide a clear understanding about the actual biology and to facilitate comparison between different scenarios.

7.1 Effects of diffusion

In general, the mobility of infectious virus particles inside the host plays some decisive roles in the progression and transmission of any kind of viral infection. In this section, in order to

Table 1: Descriptions of model variables and parameters.

Variables	Descriptions				
X	Number of uninfected hepatocytes				
Y	Number of infected hepatocytes				
U	Number of HBV DNA-containing capsids				
V	Number of viruses				
S_v	Number of SVPs				
A	Number of antibodies				
Parameters	Descriptions	Dimensional values	Units	Non-dimensional values	Source
λ	Birth rate of uninfected hepatocytes	2.6×10^7	cells $\text{ml}^{-1} \text{day}^{-1}$	0.0084	[16]
μ	Death rate of uninfected hepatocytes	0.01	day^{-1}	0.8438	[16]
k	Virus-to-cell infection rate	1.67×10^{-12}	$\text{ml virion}^{-1} \text{day}^{-1}$	1.4091	[42]
a	Production rate of capsid from infected hepatocytes	150	capsids $\text{cell}^{-1} \text{day}^{-1}$	253125	[42]
b	Production rate of SVPs from infected hepatocytes	$1000a$	capsids $\text{cell}^{-1} \text{day}^{-1}$	1468	[42]
β	Virus production rate from capsids	0.87	day^{-1}	73.40	[42]
δ	Death rate of infected hepatocyte as well as capsids	0.053	day^{-1}	4.47	[42]
δ_v	Death rate of viruses	3.8	day^{-1}	320	[42]
η	Volume fraction of HBV DNA-containing capsids	$0 \leq \alpha \leq 1$	Unitless	0.8	
γ	Recycling rate	0.6931	day^{-1}	58.21	[5]
g	Binding rate of antibody and virus or SVPs	10^{-4}	day^{-1}	8437	[43]
h	production rate of antibodies	0.01	day^{-1}	8437500	[43]
δ_s	Death rate of sub-viral particles	3.8	day^{-1}	320	Assumed
δ_a	Death rate of antibodies	0.15	day^{-1}	16.8	[43]
\mathcal{D}_1	Diffusion coefficient of capsids	0.08	$\text{cm}^2 \text{day}^{-1}$	0.0370	-
\mathcal{D}_2	Diffusion coefficient of viruses	0.09	$\text{cm}^2 \text{day}^{-1}$	0.0417	-
\mathcal{D}_3	Diffusion coefficient of SVPs	0.09	$\text{cm}^2 \text{day}^{-1}$	0.0417	-
\mathcal{D}_4	Diffusion coefficient of antibodies	0.08	$\text{cm}^2 \text{day}^{-1}$	0.0370	-

examine the relative importance of diffusion of capsids, viruses, SVPs and antibodies on HBV infection dynamics, we first consider the system in the absence of any kind of diffusion, (*i.e.*, $\mathcal{D}_1 = \mathcal{D}_2 = \mathcal{D}_3 = \mathcal{D}_4 = 0$). Subsequently, when diffusivity is imposed into the model, the values of diffusion coefficients ($\mathcal{D}_1, \mathcal{D}_2, \mathcal{D}_3, \mathcal{D}_4$) are varied within the empirically reliable range to explore diverse scenarios and uncover testable biological aspects. In this case, none of the diffusion coefficients are set to zero. We proceed in the following manner:

1. The effects of diffusion on uninfected and infected hepatocytes.
2. The effects of diffusion on HBV capsids and free viruses.
3. The effects of diffusion on SVPs and antibodies.

7.1.1 Effects of diffusion on uninfected and infected hepatocytes

The changes in the dynamics of uninfected and infected hepatocytes are shown in the Figure 4. In order to visualize the concentration profiles of respective classes with respect to time and space in a easier way, contour color plots are presented. Figure 4A and Figure 4B display the distribution pattern of uninfected hepatocytes with and without considering the diffusivity of HBV capsids, viruses, SVPs and antibodies, respectively. Significant variations are observed in the distribution patterns. At the early stages of infection, the influence of diffusion on the uninfected hepatocytes compartment is not noticeable, as the concentration remains nearly uniform across times (contour lines are parallel to space-axis). However, subsequent to this initial phase, diffusion begins to exert substantial impacts. For these set of parameters, after the time $t \approx 1330^{th}$ day, the distribution of uninfected hepatocytes shows a paradigm shift in the contour line (for example, contour line 2450000000). In the diffusion model, uninfected hepatocytes exhibit an almost uniform distribution along space, whereas in the non-diffusion model, they display a non-uniform pattern. In the non-diffusion model, the infection takes a considerable amount of time to spread throughout the liver.

In case of infected hepatocytes, similar kind of dynamics are observed in Figure 4C and Figure 4D as shown in uninfected hepatocytes. In the non-diffusion model, the rate of temporal changes in the concentration of infected hepatocytes is higher compared to diffusion one. In essence, the diffusion of virion components (capsids, virions, SVPs) and antibodies enhances the infection increasing the susceptibility in cells. However, both models lead to the same steady state for both type of hepatocytes.

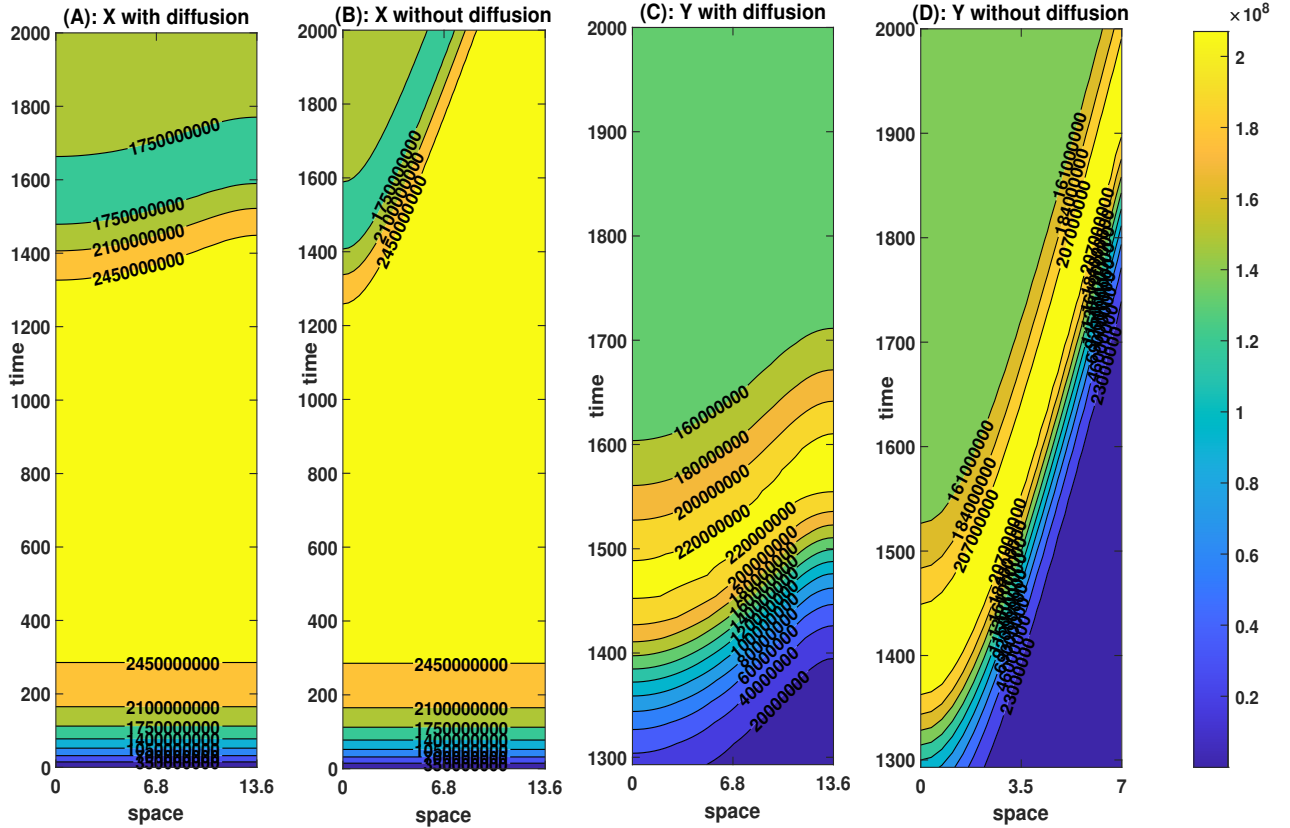


Figure 4: Contour color plots: The effects of diffusion on uninfected and infected hepatocytes.

7.1.2 Effects of diffusion on HBV capsids and free viruses

The contour plots shown in Figure 5 delineates the concentration profiles of HBV DNA-containing capsids and viruses. For non-zero values of diffusion coefficients $\mathcal{D}_1, \mathcal{D}_2, \mathcal{D}_3, \mathcal{D}_4$, the densities of capsids and viruses demonstrate an nearly orthotropic pattern (property changes in mutually perpendicular directions) in Figure 5A (capsids) and Figure 5C (viruses). It is also observed that for same time (suppose $t = 1400^{th}$ day), there are significant differences in the concentrations of capsids and viruses compartments between the diffusion and non-diffusion models. In the absence of diffusion, the spread of capsids and virion particles occurs slowly (Figure 5B and Figure 5D). However, due to the inclusion of diffusions, viruses start to propagate rapidly throughout the liver, leading to a spatially homogeneous distribution. Therefore, diffusivities of capsids, viruses, SVPs and antibodies influence the infection pattern and its dynamics.

7.1.3 Effects of diffusion on SVPs and antibodies

In this section, we discuss how the spatial movement of capsids, viruses, SVPs, and antibodies affects the concentrations of non-infectious SVPs and virus-neutralizing antibodies. In Figure 6A and Figure 6C, the values of SVPs ($S_v(x, t)$) and antibodies ($A(x, t)$) with diffusion are visualized using contour color plots. On the other hand, Figure 6B and Figure 6D shows the corresponding concentrations of SVPs and antibodies under non-diffusion conditions. Initially, it is considered that the infection starts from the left side of the liver, *i.e.*, from the origin $(0, 0)$ according to

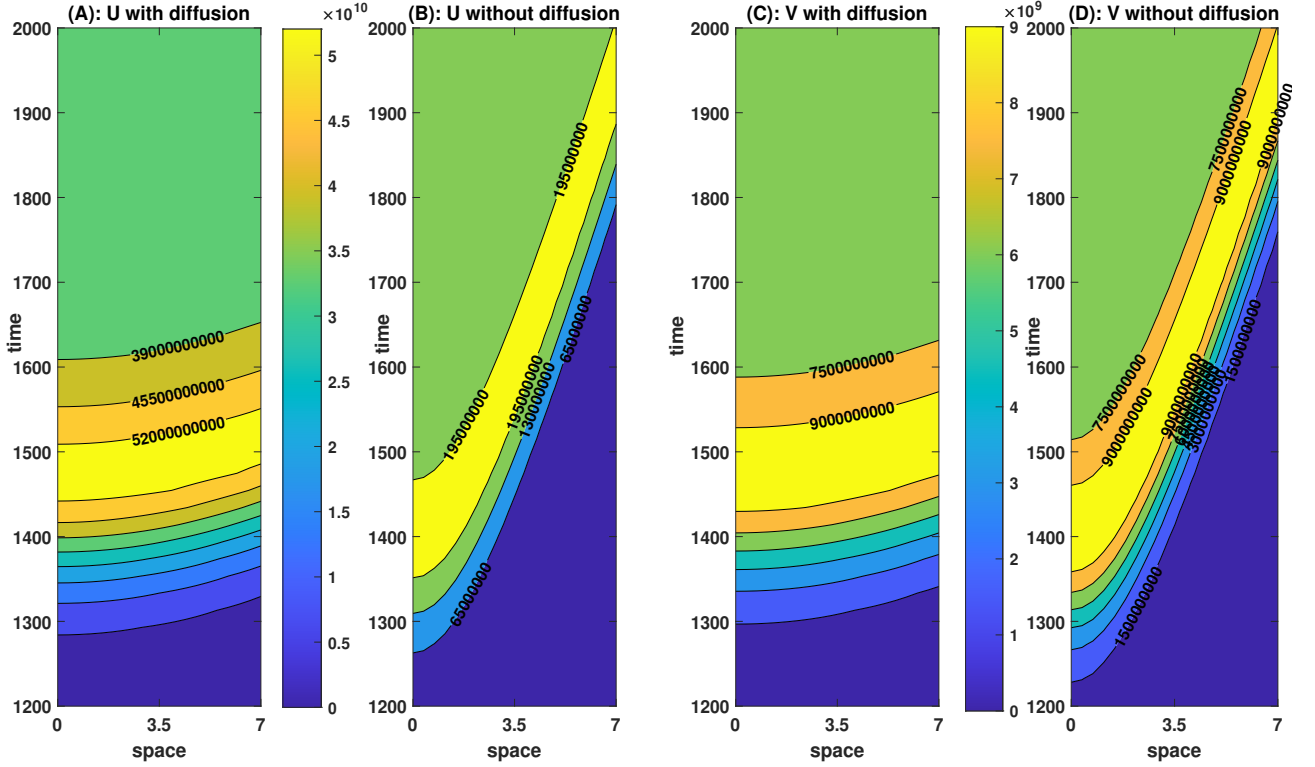


Figure 5: Contour color plots: The effects of diffusion on HBV capsids and infectious virus particles.

our xt -frame. There are notable changes in the concentrations of SVPs and antibodies observed exclusively on the left side of the liver, while the right side exhibits an absence of both SVPs and antibodies in the non-diffusion model. The antibodies are concentrated only near the site of infection in non-diffusion model. It is quite impractical. While diffusion is taken into account, substantial variations are observed occurring in both sides of the liver.

Contour plots shown in Figure 4, 5 and 6 indicate that all compartments (uninfected hepatocytes, infected hepatocytes, capsids, viruses, SVPs and antibodies) reach an endemic steady-state more rapidly in case of non-diffusion model compared to the diffusion one.

7.2 Effects of SVPs

SVPs are one of the intracellular viral components that weaken the host immune system. These viral elements release from the infected hepatocytes in a large number (typically 1,000- to 100,000-fold) compare to infectious virus particles during infection period [9–11]. In this section, we investigate the effects of SVPs on virus and antibody growth dynamics throughout the liver. The system of equations (11) (16) is solved by considering both the cases: (i) with SVPs and (ii) without SVPs. In Figure 7 (1-6), the solution for the first case *i.e.* solutions with the SVPs are displayed. On the other hand, the outcomes for the second case (without SVPs) are depicted in Figure 7 (7-12). Upon comparing the solutions for both cases, notable changes are observed, particularly in the virus and antibody profiles. The snapshots of the virus and antibody compartments are captured at different positions, such as at $x = 2.5$, $x = 5$, $x = 7.5$, $x = 10$, $x = 12.5$ and $x = 13.6$, and shown in Figure 7 (13-18) for virus and Figure 7 (19-24) for antibody. Due to the integration of SVPs into the model, these following critical insights are noted:

1. There is a discernible rise in the peak of virus compartment (refers Figure 7 (13-18)).
2. The virus compartment stabilizes at a higher level (refers Figure 7 (13-18)).

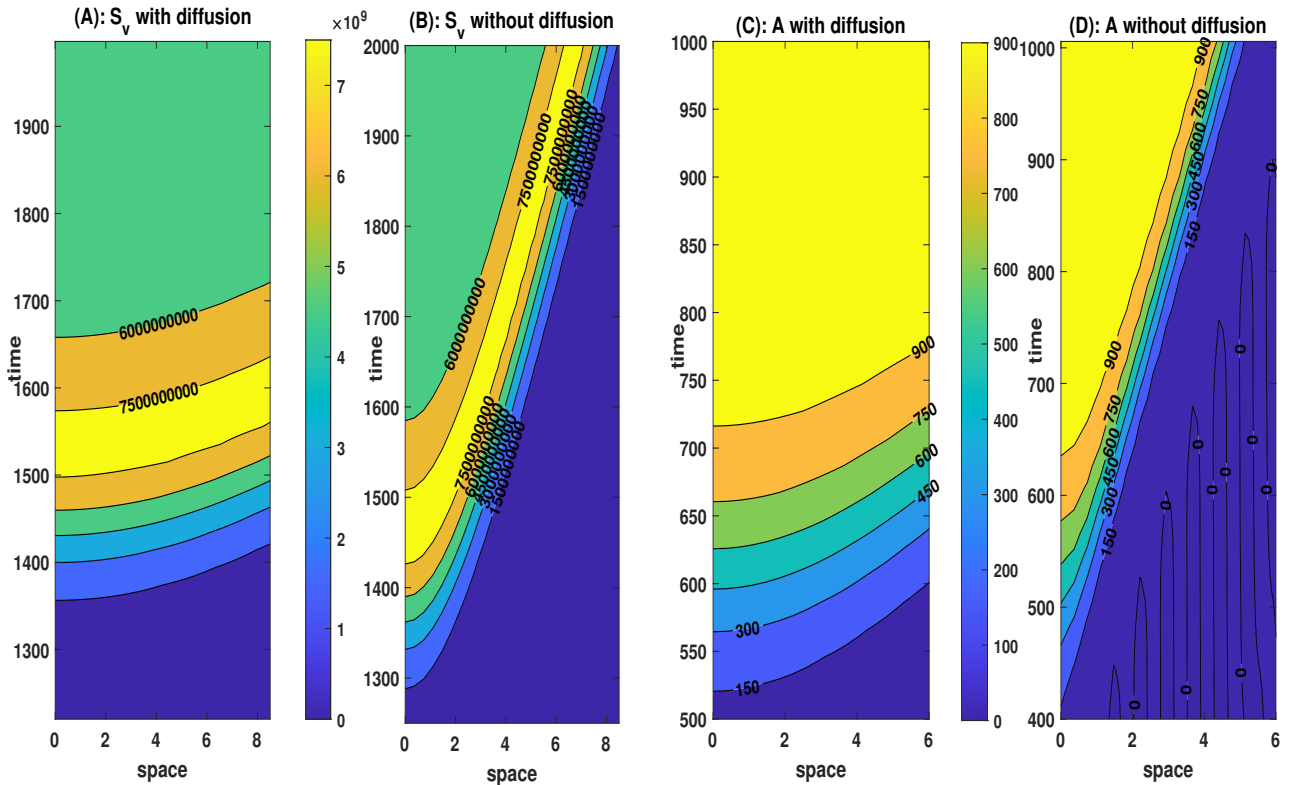


Figure 6: Contour color plots: The effects of diffusion on SVPs and antibodies.

3. The peak level for the virions compartment rises quickly (refers Figure 7 (13-18)).
4. After a certain time period, substantial changes are observed in the solution for the antibody compartment (refers Figure 7 (19-24)). The stability level of antibodies significantly decreases due to the presence of SVPs. The primary reason is the excessive production of SVPs which leads to the depletion of a considerable amount of antibodies, resulting in a swift decline in antibody concentration.

Therefore, the above findings suggest that SVPs play some important roles in development of this viral infection. Similar types of results have been reported in the literature. For example, Bruns et al. [28] found that SVPs significantly enhance intracellular viral replication and gene expression. Recently, Rydell et al. [26] confirmed that SVPs significantly reduced the neutralization of virus particles by antibodies. The removal of spherical SVPs stands as an important milestone in achieving the functional cure of HBV infection [44]. Thus, in conclusion, SVPs merit attention as a promising avenue for future therapeutic strategies targeting viral agents.

7.3 Effects of capsid recycling on the production of SVPs

The recycling of capsids acts as a crucial mechanism in HBV. Recently, Sutradhar and Dalal [24,35] found how the recycling pathway substantially augments viral concentration during HBV infection. To the best of our knowledge, we didn't find any prior documented investigations related the interplay between capsid recycling and SVPs in the literature. The possible associations between capsid recycling and SVPs are studied here. The proposed model is solved under two distinct cases:

Case-1: without recycling ($\gamma = 0, \alpha = 1$)

In this case, the impacts of capsid recycling is ignored, *i.e.*, the simulation is done by considering $\gamma = 0$ and the corresponding profiles of SVPs are shown in Figure 8A.

Case-2: with recycling ($\gamma \neq 0, \alpha < 1$)

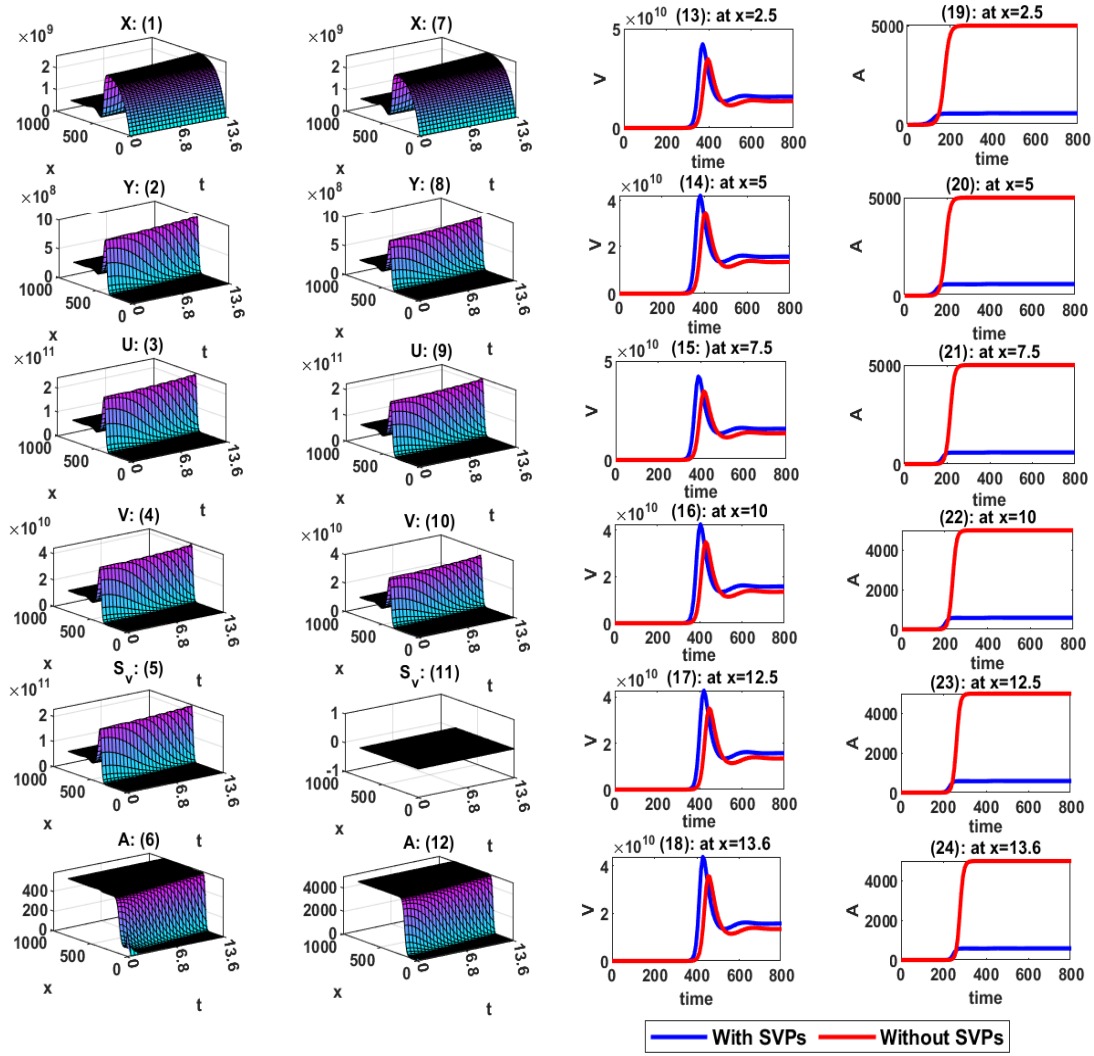


Figure 7: Comparisons between the virus and antibody profiles considering both the cases: with and without SVPs. Here, the blue lines illustrate the system's solution incorporating SVPs, while the red curves depict the solution without SVPs.

We incorporate the recycling effects into the proposed model through the term $\gamma(1 - \alpha)U(x, t)$ in equation (4). By assigning a realistic estimated value to γ , we solve the system of equations. The resulting surface plot for SVPs is depicted in Figure 8B.

In Figure 8(C)-Figure 8(H), the solutions of SVPs for various positions are highlighted. The trends of the solutions exhibit similarities but demonstrate significant differences in values. The extreme values for each solution vary considerably. Incorporation of recycling of capsids results in a higher peak in the solution compared to when recycling is not considered. Therefore, the recycling of capsids is implicated in enhancing the concentration of SVPs during HBV infection.

8 Infection initiating from multiple points on the liver

In the preceding sections, we made the assumption that the infection initially originates only from a single point at $x = 0$ (left side). Subsequently, the corresponding initial conditions were considered as described in the equation (8). This virus predominantly infects hepatocytes which serve as the primary functional cells within the liver. However, the infection doesn't necessarily involve every hepatocyte in the liver at same time. The virus may infect hepatocytes in various parts of the liver over time [45] (Figure 9). In order to explore the changes in the infection dynamics, the initial conditions (equation (8)) are modified by introducing multiple points of infection. For convenience in analyzing and comparing different scenarios, we address

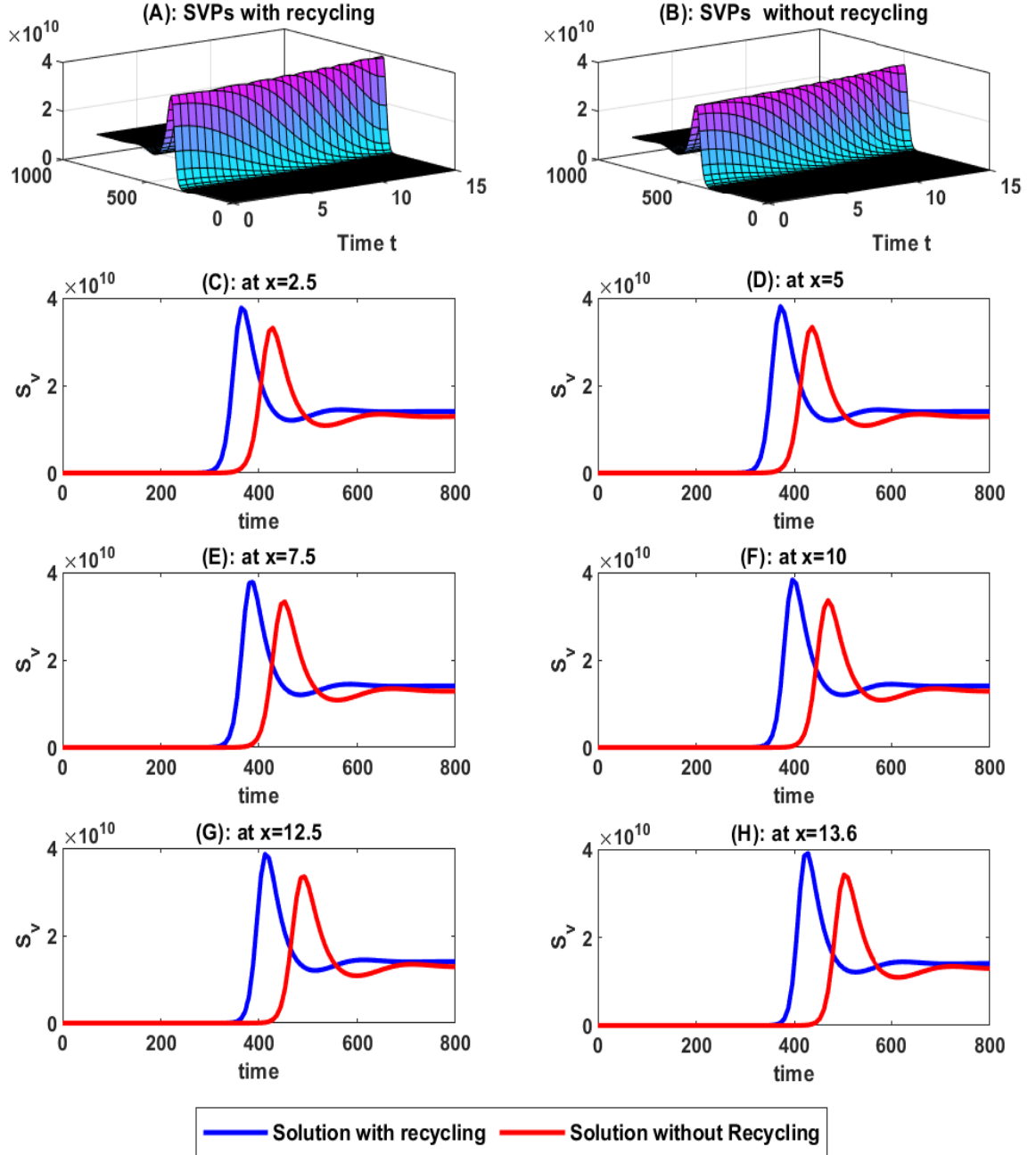


Figure 8: The effects of recycling on SVPs. Figure 8 (A): surface plot of SVPs when recycling is taken into account. Figure 8 (B): surface plot of SVPs when recycling is not considered. Figure 8 (C)-Figure 8 (H): The comparison between the concentration of SVPs at $x = 2.5$, $x = 5$, $x = 7.5$, $x = 10$, $x = 12.5$, and $x = 15$, with respect to time. Here, blue curves represent the solution of the system when recycling of capsids is considered. On the other flip, red curves denotes the solutions when recycling effects are ignored.

the solutions of the proposed model (11)-(16)

1. with single point of infection as SWSPI,
2. with dual points of infection as SWDPI,
3. with triple points of infection as SWTPI.

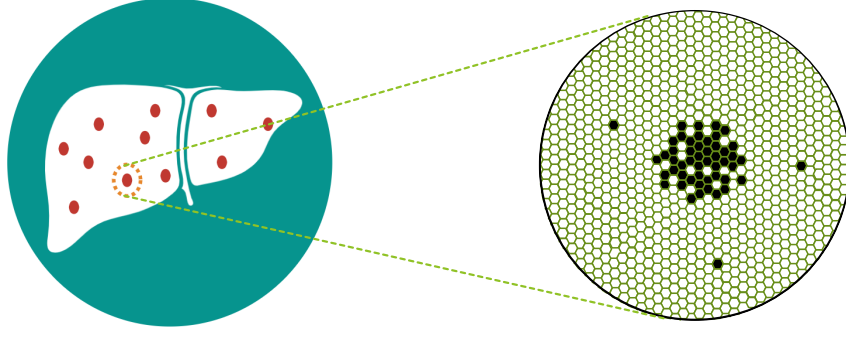


Figure 9: Distribution of infection in the liver during the course of HBV infection.

8.1 Dual-origin infection

In this case, it is assumed that the infection starts from both ends ($x = 0$ and $x = L$) of the liver with equal severity of infection. The initial numbers of infected hepatocytes, capsids, viruses, SVPs, and antibodies are considered to be same to those observed in single point infection, however, in this case, they are equally distributed into two endpoints.

8.1.1 Initial conditions

In the context of dual-origin infection, the corresponding non-dimensional form of initial conditions are given as follows:

$$\left. \begin{aligned}
 X(x, 0) &= 1 - \left\{ \exp\left(-\frac{x^2}{\epsilon^*}\right) + \exp\left(-\frac{(x-1)^2}{\epsilon^*}\right) \right\}, \quad 0 \leq x \leq 1, \\
 Y(x, 0) &= \left\{ \exp\left(-\frac{x^2}{\epsilon^*}\right) + \exp\left(-\frac{(x-1)^2}{\epsilon^*}\right) \right\}, \quad 0 \leq x \leq 1, \\
 U(x, 0) &= \left\{ \exp\left(-\frac{x^2}{\epsilon^*}\right) + \exp\left(-\frac{(x-1)^2}{\epsilon^*}\right) \right\}, \quad 0 \leq x \leq 1, \\
 V(x, 0) &= \left\{ \exp\left(-\frac{x^2}{\epsilon^*}\right) + \exp\left(-\frac{(x-1)^2}{\epsilon^*}\right) \right\}, \quad 0 \leq x \leq 1, \\
 S_v(x, 0) &= \left\{ \exp\left(-\frac{x^2}{\epsilon^*}\right) + \exp\left(-\frac{(x-1)^2}{\epsilon^*}\right) \right\}, \quad 0 \leq x \leq 1, \\
 A(x, 0) &= \left\{ \exp\left(-\frac{x^2}{\epsilon^*}\right) + \exp\left(-\frac{(x-1)^2}{\epsilon^*}\right) \right\}, \quad 0 \leq x \leq 1.
 \end{aligned} \right\} \quad (33)$$

In Figure 10, the initial state of each compartment is displayed for dual origin infection.

8.2 Triple-origin infection

Here, we consider that the liver is initially infected at three distinct points: both endpoints ($x = 0$ and $x = L$) and the midpoint ($x = L/2$). Similarly, as dual-origin infection, the total number of uninfected hepatocytes, infected hepatocytes, capsids, viruses, SVPs, and antibodies mirror those in a single-point infection.

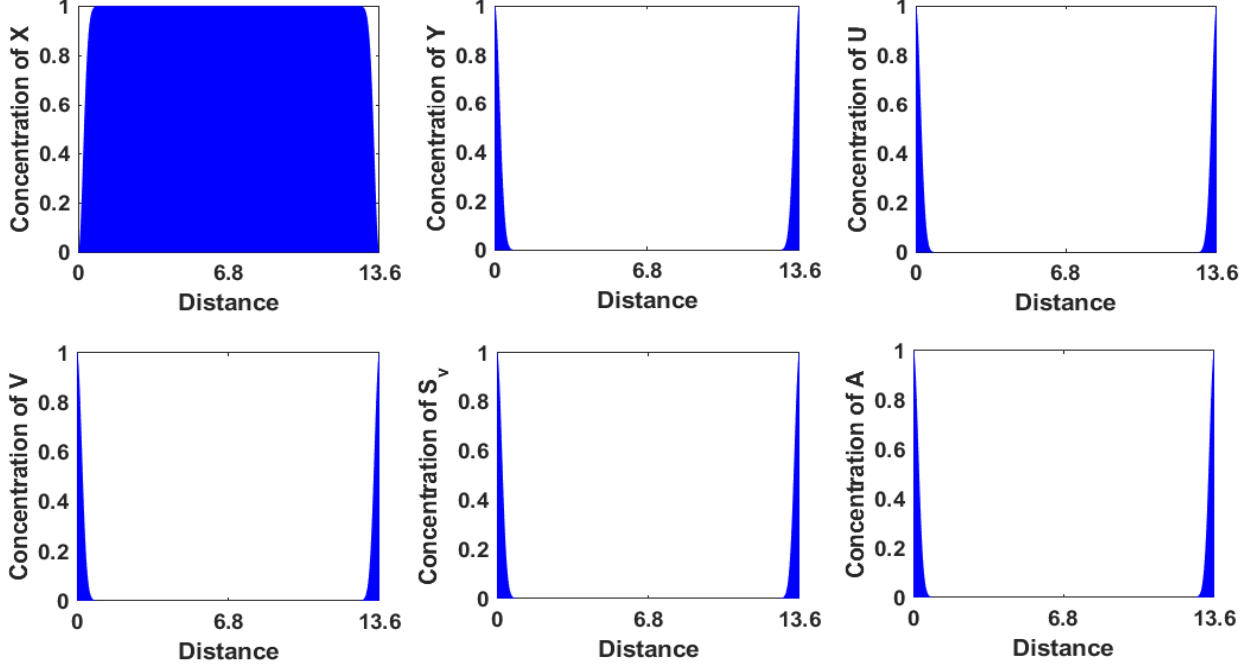


Figure 10: Initial conditions: The infection initiates at $x = 0$ and $x = L$ simultaneously.

8.2.1 Initial conditions

$$X(x, 0) = 1 - \left\{ \exp\left(-\frac{x^2}{\epsilon^*}\right) + \exp\left(-\frac{(x-0.5)^2}{\epsilon^*}\right) + \exp\left(-\frac{(x-1)^2}{\epsilon^*}\right) \right\}, \quad 0 \leq x \leq 1, \quad (34)$$

$$Y(x, 0) = \left\{ \exp\left(-\frac{x^2}{\epsilon^*}\right) + \exp\left(-\frac{(x-0.5)^2}{\epsilon^*}\right) + \exp\left(-\frac{(x-1)^2}{\epsilon^*}\right) \right\}, \quad 0 \leq x \leq 1, \quad (35)$$

$$U(x, 0) = \left\{ \exp\left(-\frac{x^2}{\epsilon^*}\right) + \exp\left(-\frac{(x-0.5)^2}{\epsilon^*}\right) + \exp\left(-\frac{(x-1)^2}{\epsilon^*}\right) \right\}, \quad 0 \leq x \leq 1, \quad (36)$$

$$V(x, 0) = \left\{ \exp\left(-\frac{x^2}{\epsilon^*}\right) + \exp\left(-\frac{(x-0.5)^2}{\epsilon^*}\right) + \exp\left(-\frac{(x-1)^2}{\epsilon^*}\right) \right\}, \quad 0 \leq x \leq 1, \quad (37)$$

$$S_v(x, 0) = \left\{ \exp\left(-\frac{x^2}{\epsilon}\right) + \exp\left(-\frac{(x-0.5)^2}{\epsilon}\right) + \exp\left(-\frac{(x-1)^2}{\epsilon}\right) \right\}, \quad 0 \leq x \leq 1, \quad (38)$$

$$A(x, 0) = \left\{ \exp\left(-\frac{x^2}{\epsilon^*}\right) + \exp\left(-\frac{(x-0.5)^2}{\epsilon^*}\right) + \exp\left(-\frac{(x-1)^2}{\epsilon^*}\right) \right\}, \quad 0 \leq x \leq 1. \quad (39)$$

(40)

Figure 11 presents the initial state of each compartment for the triple-origin infection setup.

8.2.2 Outcomes of the infection: Comparison among SWSPI, SWDPI, and SWTPI

The proposed model is solved for different initial conditions: (i) single-origin infection (17), (ii) dual-origin infection (33), and (iii) triple-origin infection (34). In order to compare the model solutions, we obtain the solution for uninfected hepatocytes, infected hepatocytes, viruses and

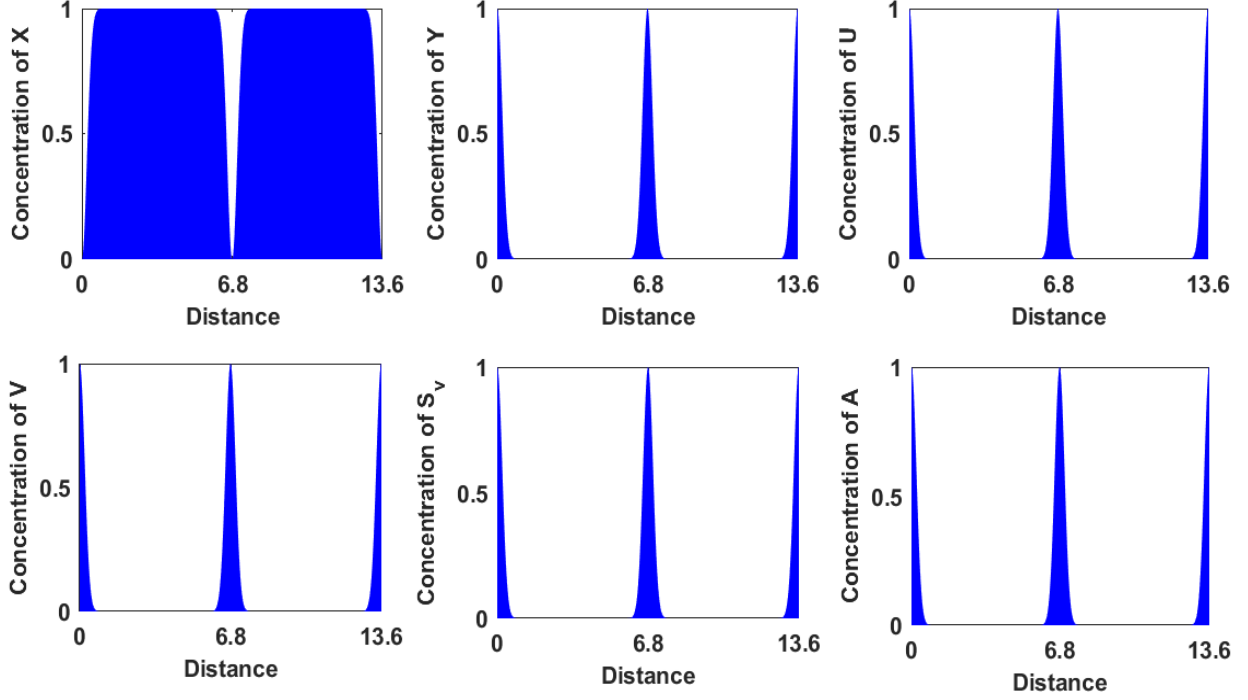


Figure 11: Initial conditions: The infection initiates at $x = 0$, $x = L/2$ and $x = L$ simultaneously.

SVPs by integrating along the spatial dimension as follows:

$$\bar{X}(t) = \int_{x=0}^{x=L} X(x, t) dx, \quad (41)$$

$$\bar{Y}(t) = \int_{x=0}^{x=L} Y(x, t) dx, \quad (42)$$

$$\bar{U}(t) = \int_{x=0}^{x=L} U(x, t) dx, \quad (43)$$

$$\bar{V}(t) = \int_{x=0}^{x=L} V(x, t) dx, \quad (44)$$

$$\bar{S}_v(t) = \int_{x=0}^{x=L} S_v(x, t) dx, \quad (45)$$

$$\bar{A}(t) = \int_{x=0}^{x=L} A(x, t) dx, \quad (46)$$

where $\bar{X}(t)$, $\bar{Y}(t)$, $\bar{V}(t)$, $\bar{S}_v(t)$ denotes the number of uninfected hepatocytes, infected hepatocytes, viruses and SVPs at time t , respectively. As the proposed model is solved numerically, the integrations (41), (42), (44), (45) are converted to summation, resulting in the following

expressions:

$$\bar{X}(t_j) = \sum_{i=1}^n X(x_n, t_j), \quad j = 1, 2, \dots, m, \quad (47)$$

$$\bar{Y}(t_j) = \sum_{i=1}^n Y(x_n, t_j), \quad j = 1, 2, \dots, m, \quad (48)$$

$$\bar{U}(t_j) = \sum_{i=1}^n U(x_n, t_j), \quad j = 1, 2, \dots, m, \quad (49)$$

$$\bar{V}(t_j) = \sum_{i=1}^n V(x_n, t_j), \quad j = 1, 2, \dots, m, \quad (50)$$

$$\bar{S}_v(t_j) = \sum_{i=1}^n S_v(x_n, t_j), \quad j = 1, 2, \dots, m, \quad (51)$$

$$\bar{A}(t_j) = \sum_{i=1}^n A(x_n, t_j), \quad j = 1, 2, \dots, m, \quad (52)$$

where n and m represent the number of grid points along x and t -axis, respectively. In Figure 12, the model solutions for uninfected hepatocytes, infected hepatocytes, viruses and SVPs are plotted and compared with each other.

- **Changes in the dynamics of uninfected hepatocytes, infected hepatocytes, viruses and SVPs**

1. The solutions converge to the same steady-state for all these three types of initial conditions.
2. As the number of initial points of infection increases, the peaks of infected hepatocytes, viruses and SVPs become higher.
3. If the liver is initially infected at multiple points, the number of infected cells increases rapidly for certain period of time from the time of infection.
4. For a triple-point infection, the solution peaks occur earlier compared to the peaks observed in solutions derived from dual-point or single-point infections.
5. From a long-term perspective, the severity of the infection remains the same regardless of the number of infection points.

9 Conclusions

In this article, a novel HBV infection dynamics model is proposed including the impacts of sub-viral particles and antibodies. The diffusivity of each viral component (capsids, viruses, SVPs) and the HBV-specific antibodies are also incorporated into the model. Overall, this model carry unique characteristics in the context of HBV infection. We perform non-dimensionalization on each model equation to make them easy in use. We apply forward time and centered space (FTCS) difference scheme to solve the proposed model numerically. Based on the experiments, this study has yielded several key findings which are as follows:

1. SVPs significantly enhance intracellular viral replication and gene expression. SVPs also reduce the neutralization of virus particles by antibodies.
2. Due to the substantial presence of SVPs within the liver, the virions compartment experiences a rapid increase and leads to a higher peak level. The stability level of virions also increases due to the incorporation of SVPs.
3. The recycling of capsids significantly enhances the concentration of SVPs.

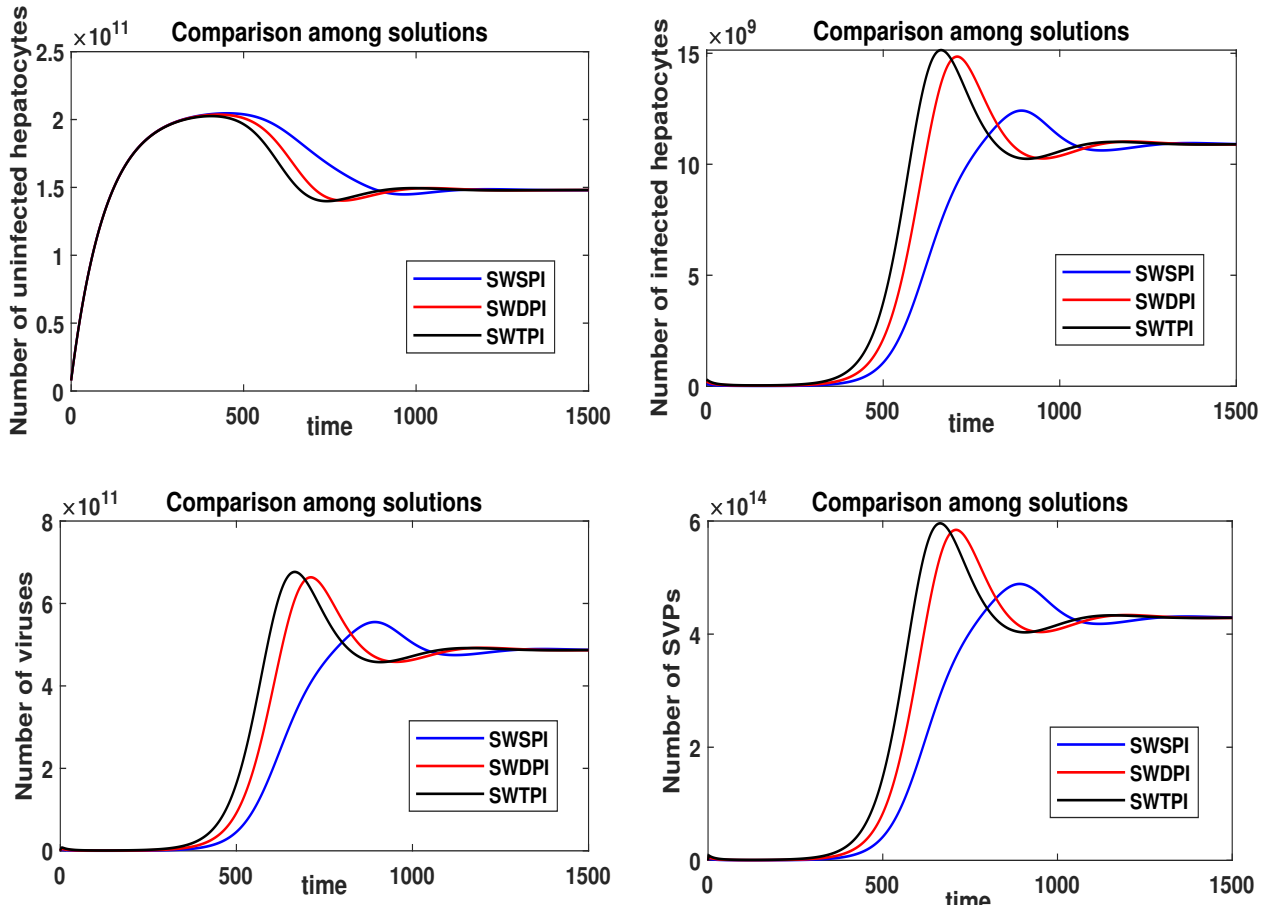


Figure 12: Comparison between solutions SWSPI, SWDPI and SWTPI. SWSPI: solution with single point infection, SWDPI: solution with double points infection, SWTPI: solution with triple points infection.

4. Due to the diffusion of capsids, viruses, SVPs and antibodies, viruses spread rapidly throughout the liver. However, all model compartments ultimately converge to the same steady-state, regardless of whether diffusion is considered or not within the model.
5. As the number of initial points of infection increases, the peaks of infected hepatocytes, viruses and SVPs become higher and occur earlier.
6. From a long-term perspective, the severity of the infection remains the same regardless of the number of infection points.

This model offers a theoretical framework for understanding the mechanism behind the exacerbation during chronic HBV infection. This model enhances our ability to accurately depict the dynamics of the infection. This model holds promise for practical application once the clinical trials are done.

Acknowledgments

First author would like to acknowledge the financial support obtained from CSIR (New Delhi) under the CSIR-SRF Fellowship scheme (File No: 09/731(0171)/2019-EMR-I). The second author of this article thanks to Ministry of Education, Govt. of India for research fellowship and Indian Institute of Technology Guwahati, India for the support provided during the period of this work. All authors thank the research facilities received from the Department of Mathematics, Indian Institute of Technology Guwahati, India.

Author contributions

All authors contribute equally.

Conflict of interest

The authors declare no potential conflict of interests.

Data Availability Statement

Data sharing is not applicable to this article.

References

- [1] Hepatitis b. <https://www.who.int/news-room/fact-sheets/detail/hepatitis-b>. 27 July 2021.
- [2] Lequan Min, Yongmei Su, and Yang Kuang. Mathematical analysis of a basic virus infection model with application to hbv infection. *The Rocky Mountain Journal of Mathematics*, 38(5):1573–1585, 2008.
- [3] Jun Nakabayashi. The intracellular dynamics of hepatitis b virus (hbv) replication with reproduced virion “re-cycling”. *Journal of Theoretical Biology*, 396:154–162, 2016.
- [4] F Fatehi Chenar, YN Kyrychko, and KB Blyuss. Mathematical model of immune response to hepatitis b. *Journal of Theoretical Biology*, 447:98–110, 2018.
- [5] John M Murray and Ashish Goyal. In silico single cell dynamics of hepatitis b virus infection and clearance. *Journal of Theoretical Biology*, 366:91–102, 2015.
- [6] Stanca M Ciupe, Naveen K Vaidya, and Jonathan E Forde. Early events in hepatitis b infection: the role of inoculum dose. *Proceedings of the Royal Society B*, 288(1944):20202715, 2021.
- [7] Georgia-Myrto Prifti, Dimitrios Moianos, Erofli Giannakopoulou, Vasiliki Pardali, John E Tavis, and Grigoris Zoidis. Recent advances in hepatitis b treatment. *Pharmaceuticals*, 14(5):417, 2021.
- [8] Philippe Gripon, Isabelle Cannie, and Stephan Urban. Efficient inhibition of hepatitis b virus infection by acylated peptides derived from the large viral surface protein. *Journal of virology*, 79(3):1613–1622, 2005.
- [9] Wolfram H Gerlich. Medical virology of hepatitis b: how it began and where we are now. *Virology journal*, 10(1):1–25, 2013.
- [10] L Luckenbaugh, KM Kitrinis, WE Delaney IV, and J Hu. Genome-free hepatitis b virion levels in patient sera as a potential marker to monitor response to antiviral therapy. *Journal of viral hepatitis*, 22(6):561–570, 2015.
- [11] Jianming Hu and Kuancheng Liu. Complete and incomplete hepatitis b virus particles: formation, function, and application. *Viruses*, 9(3):56, 2017.
- [12] Tamako Garcia, Jisu Li, Camille Sureau, Kiyooki Ito, Yanli Qin, Jack Wands, and Shuping Tong. Drastic reduction in the production of subviral particles does not impair hepatitis b virus virion secretion. *Journal of virology*, 83(21):11152–11165, 2009.

- [13] Martin A Nowak, Sebastian Bonhoeffer, Andrew M Hill, Richard Boehme, Howard C Thomas, and Hugh McDade. Viral dynamics in hepatitis b virus infection. *Proceedings of the National Academy of Sciences*, 93(9):4398–4402, 1996.
- [14] John M Murray, Stefan F Wieland, Robert H Purcell, and Francis V Chisari. Dynamics of hepatitis b virus clearance in chimpanzees. *Proceedings of the National Academy of Sciences*, 102(49):17780–17785, 2005.
- [15] Stanca M Ciupe, Ruy M Ribeiro, Patrick W Nelson, Geoffrey Dusheiko, and Alan S Perelson. The role of cells refractory to productive infection in acute hepatitis b viral dynamics. *Proceedings of the National Academy of Sciences*, 104(12):5050–5055, 2007.
- [16] Harel Dahari, Arthur Lo, Ruy M Ribeiro, and Alan S Perelson. Modeling hepatitis c virus dynamics: Liver regeneration and critical drug efficacy. *Journal of Theoretical Biology*, 247(2):371–381, 2007.
- [17] Kaifa Wang and Wendi Wang. Propagation of hbv with spatial dependence. *Mathematical Biosciences*, 210(1):78–95, 2007.
- [18] Steffen Eikenberry, Sarah Hews, John D Nagy, and Yang Kuang. The dynamics of a delay model of hbv infection with logistic hepatocyte growth. *Mathematical Biosciences and Engineering*, 6:1–17, 2009.
- [19] Sarah Hews, Steffen Eikenberry, John D Nagy, and Yang Kuang. Rich dynamics of a hepatitis b viral infection model with logistic hepatocyte growth. *Journal of Mathematical Biology*, 60(4):573–590, 2010.
- [20] Jun Nakabayashi and Akira Sasaki. A mathematical model of the intracellular replication and within host evolution of hepatitis type b virus: Understanding the long time course of chronic hepatitis. *Journal of Theoretical Biology*, 269(1):318–329, 2011.
- [21] Jaouad Danane and Karam Allali. Mathematical analysis and treatment for a delayed hepatitis b viral infection model with the adaptive immune response and dna-containing capsids. *High-throughput*, 7(4):35, 2018.
- [22] Ting Guo, Haihong Liu, Chenglin Xu, and Fang Yan. Global stability of a diffusive and delayed hbv infection model with hbv dna-containing capsids and general incidence rate. *Discrete & Continuous Dynamical Systems-B*, 23(10):4223, 2018.
- [23] Farzad Fatehi, Richard J Bingham, Eric C Dykeman, Nikesh Patel, Peter G Stockley, and Reidun Twarock. An intracellular model of hepatitis b viral infection: An in silico platform for comparing therapeutic strategies. *Viruses*, 13(1):11, 2021.
- [24] Rupchand Sutradhar and D. C. Dalal. Fractional-order models of hepatitis b virus infection with recycling effects of capsids. *Mathematical Methods in the Applied Sciences*, 46(14):15599–15625.
- [25] Jianhao Cao, Junchang Zhang, Yanmeng Lu, Shuhong Luo, Jingqiang Zhang, and Ping Zhu. Cryo-em structure of native spherical subviral particles isolated from hbv carriers. *Virus research*, 259:90–96, 2019.
- [26] Gustaf E Rydell, Kasthuri Prakash, Heléne Norder, and Magnus Lindh. Hepatitis b surface antigen on subviral particles reduces the neutralizing effect of anti-hbs antibodies on hepatitis b viral particles in vitro. *Virology*, 509:67–70, 2017.
- [27] Ning Chai, Ho Eun Chang, Emmanuelle Nicolas, Ziyang Han, Michal Jarnik, and John Taylor. Properties of subviral particles of hepatitis b virus. *Journal of virology*, 82(16):7812–7817, 2008.

- [28] Michael Bruns, Stefan Miska, Sylvie Chassot, and Hans Will. Enhancement of hepatitis b virus infection by noninfectious subviral particles. *Journal of virology*, 72(2):1462–1468, 1998.
- [29] U Klingmüller and H Schaller. Hepadnavirus infection requires interaction between the viral pre-s domain and a specific hepatocellular receptor. *Journal of Virology*, 67(12):7414–7422, 1993.
- [30] Peng Wu and Hongyong Zhao. Dynamical analysis of a nonlocal delayed and diffusive hiv latent infection model with spatial heterogeneity. *Journal of the Franklin Institute*, 358(10):5552–5587, 2021.
- [31] Peng Wu, Xiunan Wang, and Zhaosheng Feng. Spatial and temporal dynamics of sars-cov-2: Modeling, analysis and simulation. *Applied mathematical modelling*, 113:220–240, 2023.
- [32] Hui Miao, Meiyang Jiao, et al. Dynamics of a diffusive hbv infection model with capsids, two delays, and cell-to-cell transmissions. *Discrete Dynamics in Nature and Society*, 2023, 2023.
- [33] Rui Xu and Zhien Ma. An hbv model with diffusion and time delay. *Journal of Theoretical Biology*, 257(3):499–509, 2009.
- [34] Kaifa Wang, Wendi Wang, and Shiping Song. Dynamics of an hbv model with diffusion and delay. *Journal of Theoretical Biology*, 253(1):36–44, 2008.
- [35] Rupchand Sutradhar and D. C. Dalal. Re-cycling of dna-containing capsids enhances hepatitis b.
- [36] Reinhild Prange. Host factors involved in hepatitis b virus maturation, assembly, and egress. *Medical microbiology and immunology*, 201(4):449–461, 2012.
- [37] Stanca M Ciupe, Ruy M Ribeiro, and Alan S Perelson. Antibody responses during hepatitis b viral infection. *PLoS computational biology*, 10(7):e1003730, 2014.
- [38] F Fatehi Chenar, YN Kyrychko, and KB Blyuss. Mathematical model of immune response to hepatitis b. *Journal of theoretical biology*, 447:98–110, 2018.
- [39] Kuo-Sheng Huang, Yu-Chiau Shyu, Chih-Lang Lin, and Feng-Bin Wang. Mathematical analysis of an hbv model with antibody and spatial heterogeneity. *Math. Biosci. Eng*, 17(2):1820–1837, 2019.
- [40] Mark AJ Chaplain and G Lolas. Mathematical modelling of cancer invasion of tissue: dynamic heterogeneity. *Networks Heterog. Media*, 1(3):399–439, 2006.
- [41] Kamrul Islam. Role of ultrasonography to detect liver size. *Ultrasound in Medicine and Biology*, 45:S96, 2019.
- [42] John M Murray, Robert H Purcell, and Stefan F Wieland. The half-life of hepatitis b virions. *Hepatology*, 44(5):1117–1121, 2006.
- [43] Adil Meskaf, Karam Allali, and Youssef Tabit. Optimal control of a delayed hepatitis b viral infection model with cytotoxic t-lymphocyte and antibody responses. *International Journal of Dynamics and Control*, 5:893–902, 2017.
- [44] Andrew Vaillant. Hbsag, subviral particles, and their clearance in establishing a functional cure of chronic hepatitis b virus infection. *ACS infectious diseases*, 7(6):1351–1368, 2020.
- [45] Andrew Vaillant. Transaminase elevations during treatment of chronic hepatitis b infection: Safety considerations and role in achieving functional cure. *Viruses*, 13(5):745, 2021.